

Electromagnetic Structure of the Nucleon in the Perturbative Chiral Quark Model

V. E. Lyubovitskij ^{*†}, Th. Gutsche ^{*} and Amand Faessler ^{*}

^{*} *Institut für Theoretische Physik, Universität Tübingen, Auf der Morgenstelle 14,
D-72076 Tübingen, Germany*

[†] *Department of Physics, Tomsk State University, 634050 Tomsk, Russia*

Abstract

We apply the perturbative chiral quark model (PCQM) at one loop to analyse the electromagnetic structure of nucleons. This model is based on an effective Lagrangian, where baryons are described by relativistic valence quarks and a perturbative cloud of Goldstone bosons. Including the electromagnetic interaction we first develop the formalism up to one-loop in the Goldstone boson fluctuation relying on renormalization by use of counterterms. Local gauge invariance is satisfied both on the Lagrangian level and also for the relevant baryon matrix elements in the Breit frame. We apply the formalism to obtain analytical expressions for the nucleon charge and magnetic form factors, which are expressed in terms of fundamental parameters of low-energy pion-nucleon physics (weak pion decay constant, axial nucleon coupling, strong pion-nucleon form factor) and of only one model parameter (radius of the nucleonic three-quark core). A detailed numerical analysis for the nucleon magnetic moments, charge and magnetic radii and also for the momentum dependence of form factors is presented.

PACS: 11.10.Ef, 12.39.Fe, 12.39.Ki, 13.40.Em, 13.40.Gp, 14.20.Dh

Keywords: Chiral symmetry; Relativistic quark model; Relativistic effective Lagrangian; Nucleon electromagnetic form factors.

I. INTRODUCTION

The study of the electromagnetic form factors of the nucleon is of fundamental importance in hadron physics to gain a deeper understanding of the baryon structure and the interplay between strong and electromagnetic interactions. Completed and ongoing experiments at ELSA, JLab, MAMI, MIT, NIKHEF and other laboratories on improved measurements of the elastic proton and neutron form factors stimulated a comprehensive

theoretical study of these quantities. The theoretical description of electromagnetic form factors was performed in detail within different approaches of low-energy hadron physics: QCD Sum Rules, Chiral Perturbation Theory, relativistic and non-relativistic quark models, QCD-motivated approaches based on solutions of the Schwinger-Dyson/Bethe-Salpeter and Faddeev equations, soliton-type models, etc. For recent experimental and theoretical advances with respect to the electromagnetic structure of nucleons see the proceedings of the last conferences [1]- [3].

Since the early eighties chiral quark models [4]- [8], describing the nucleon as a bound system of valence quarks with a surrounding pion cloud, play an important role in the description of low-energy nucleon physics. These models include the two main features of low-energy hadron structure, confinement and chiral symmetry. With respect to the treatment of the pion cloud these approaches fall essentially into two categories.

The first type of chiral quark models assumes that the valence quark content dominates the nucleon, thereby treating pion contributions perturbatively [4-6,8]. Originally, this idea was formulated in the context of the cloudy bag model [4]. By imposing chiral symmetry the MIT bag model [9] was extended to include the interaction of the confined quarks with the pion fields on the bag surface. With the pion cloud treated as a perturbation on the basic features of the MIT bag, pionic effects generally improve the description of nucleon observables. Later, similar perturbative chiral models [5,6,8] were developed where the rather unphysical sharp bag boundary is replaced by a finite surface thickness of the quark core. By introducing a static quark potential of general form, these quark models contain a set of free parameters characterizing the confinement (coupling strength) and/or the quark masses. The perturbative technique allows a fully quantized treatment of the pion field up to a given order in accuracy. Although formulated on the quark level, where confinement is put in phenomenologically, perturbative chiral quark models are formally close to chiral perturbation theory on the hadron level.

Alternatively, when the pion cloud is assumed to dominate the nucleon structure this effect has to be treated non-perturbatively. The non-perturbative approaches are based for example on Refs. [7], where the chiral quark soliton model was derived. This model is based on the concept that the QCD instanton vacuum is responsible for the spontaneous breaking of chiral symmetry, which in turn leads to an effective chiral Lagrangian at low energy as "derived" from QCD. The classical pion field (the soliton) is described by a trial profile function, which is fixed by minimizing the energy of the nucleon. Further quantization of slow rotations of this soliton field leads to a nucleon state, which is built up from rotational excitations of the classical nucleon. On the phenomenological level the chiral quark soliton model tends to be advantageous in the description of the nucleon spin structure, that is for large momentum transfers, but is comparable to the original perturbative chiral quark models in the description of low-energy nucleon properties.

As a further development of chiral quark models with a perturbative treatment of the pion cloud [4-6,8], we extended the relativistic quark model suggested in [8] for the study of the low-energy properties of the nucleon [10]. Compared to the previous similar models of Refs. [4-6] our current approach contains several new features: i) generalization of the phenomenological confining potential; ii) SU(3) extension of chiral symmetry to include the kaon and eta-meson cloud contributions; iii) consistent formulation of perturbation theory both on the quark and baryon level by use of renormalization techniques and by allowing

to account for excited quark states in the meson loop diagrams; iv) fulfillment of the constraints imposed by chiral symmetry (low-energy theorems), including the current quark mass expansion of the matrix elements (for details see Ref. [10]); v) possible consistency with chiral perturbation theory as for example demonstrated [10] for the chiral expansion of the nucleon mass. In the following we refer to our model as the *perturbative chiral quark model* (PCQM).

The PCQM is based on an effective chiral Lagrangian describing quarks as relativistic fermions moving in a self-consistent field (static potential). The latter is described by a scalar potential S providing confinement of quarks and the time component of a vector potential $\gamma^0 V$ responsible for short-range fluctuations of the gluon field configurations [11] (see also recent lattice calculations [12]). The model potential defines unperturbed wave functions of quarks which are subsequently used in the calculation of baryon properties. Baryons in the PCQM are described as bound states of valence quarks surrounded by a cloud of Goldstone bosons (π, K, η) as required by chiral symmetry. Interaction of quarks with Goldstone bosons is introduced on the basis of the nonlinear σ -model [13]. When considering mesons fields as small fluctuations we restrict ourselves to the linear form of the meson-quark interaction. With the derived interaction Lagrangian we do our perturbation theory in the expansion parameter $1/F$ (where F is the pion leptonic decay constant in the chiral limit). We also treat the mass term of the current quarks as a small perturbation. Dressing the baryon three-quark core by a cloud of Goldstone mesons corresponds to the inclusion of the sea-quark contribution. All calculations are performed at one loop or at order of accuracy $o(1/F^2, \hat{m}, m_s)$. The chiral limit with $\hat{m}, m_s \rightarrow 0$ is well defined.

In Ref. [10] our approach was successfully applied to the study of sigma-term physics. Our result for the πN sigma term $\sigma_{\pi N} \approx 45$ MeV is in good agreement with the value deduced by Gasser, Leutwyler and Sainio [14] using dispersion-relation techniques and exploiting the chiral symmetry constraints. A complete analysis of meson-nucleon and meson-delta-isobar sigma-terms, is given including the strangeness content of the nucleon. We have a physically reasonable prediction for the quantity $y_N = 0.076 \pm 0.012$ [10] characterizing the strange quark contribution to the nucleon mass. Our predictions for the strangeness content of the nucleon and for KN sigma-terms are important for the ongoing DAΦNE experiments at Frascati [15].

In this paper, we apply the PCQM to analyse the electromagnetic structure of nucleons. The main intention of the present work is to develop the full formalism for the effective Lagrangian of the PCQM, where Goldstone boson fluctuations are treated as higher order effects to the pure valence quark core results. We give detailed consideration of gauge invariance in noncovariant chiral quark model treating pion cloud perturbatively.

In the present article we proceed as follows. In the following section, we first describe the basic notions of our approach: the underlying effective Lagrangian, choice of parameters and fulfillment of low-energy theorems. We extend our model Lagrangian by including the electromagnetic interaction. A consistent formalism of the perturbation series up to one meson loop and up to terms linear in the current quark masses is presented. We utilize a renormalization technique, which, by introducing counterterms, greatly simplifies the evaluation. Thereby, local gauge invariance of the electromagnetic interaction is shown to be fulfilled both on the Lagrangian level and for baryon matrix elements set up in the Breit frame. In Sect. 3 we concentrate on the specific application of the PCQM to the electromagnetic properties

of the nucleon. We derive analytical expressions for the nucleon charge and magnetic form factors expressed in terms of fundamental parameters of low-energy pion-nucleon physics (weak pion decay constant, axial nucleon coupling, strong pion-nucleon form factor) and of only one model parameter (radius of the nucleonic three-quark core). Numerical results in comparison with data are presented to test the basic and standard phenomenological implications of the model. Finally, Sect. 4 contains a summary of our major conclusions.

II. PERTURBATIVE CHIRAL QUARK MODEL

A. Effective Lagrangian and zeroth order properties

The perturbative chiral quark model (PCQM) [10] is based on an effective chiral Lagrangian describing the valence quarks of baryons as relativistic fermions moving in a self-consistent field (static potential) $V_{eff}(r) = S(r) + \gamma^0 V(r)$ with $r = |\vec{x}|$ [8,5,16], which are supplemented by a cloud of Goldstone bosons (π, K, η). Treating Goldstone fields as small fluctuations around the three-quark (3q) core we derive a linearized effective Lagrangian \mathcal{L}_{eff} . The Lagrangian $\mathcal{L}_{eff} = \mathcal{L}_{inv}^{lin} + \mathcal{L}_{\chi SB}$, derived in Ref. [10], includes the linear chiral-invariant term

$$\mathcal{L}_{inv}^{lin}(x) = \bar{\psi}(x)[i \not{\partial} - S(r) - \gamma^0 V(r)]\psi(x) + \frac{1}{2}(\partial_\mu \hat{\Phi}(x))^2 - \bar{\psi}(x)S(r)i\gamma^5 \frac{\hat{\Phi}(x)}{F}\psi(x) \quad (1)$$

and a term $\mathcal{L}_{\chi SB}$ which explicitly breaks chiral symmetry

$$\mathcal{L}_{\chi SB}(x) = -\bar{\psi}(x)\mathcal{M}\psi(x) - \frac{B}{8}\text{Tr}\{\hat{\Phi}(x), \{\hat{\Phi}(x), \mathcal{M}\}\} \quad (2)$$

containing the mass terms for quarks and mesons [10]. The octet matrix $\hat{\Phi}$ of pseudoscalar mesons is defined as:

$$\frac{\hat{\Phi}}{\sqrt{2}} = \sum_{i=1}^8 \frac{\Phi_i \lambda_i}{\sqrt{2}} = \begin{pmatrix} \pi^0/\sqrt{2} + \eta/\sqrt{6} & \pi^+ & K^+ \\ \pi^- & -\pi^0/\sqrt{2} + \eta/\sqrt{6} & K^0 \\ K^- & \bar{K}^0 & -2\eta/\sqrt{6} \end{pmatrix}; \quad (3)$$

$F = 88$ MeV [10,17] is the pion decay constant in the chiral limit; $\mathcal{M} = \text{diag}\{\hat{m}, \hat{m}, m_s\}$ is the mass matrix of current quarks¹; $B = -\langle 0|\bar{u}u|0\rangle / F^2$ is the low-energy constant which measures the vacuum expectation value of the scalar quark densities in the chiral limit [18]. We rely on the standard picture of chiral symmetry breaking [18] and for the masses of pseudoscalar mesons we use the leading term in their chiral expansion (i.e. linear in the current quark mass):

$$M_\pi^2 = 2\hat{m}B, \quad M_K^2 = (\hat{m} + m_s)B, \quad M_\eta^2 = \frac{2}{3}(\hat{m} + 2m_s)B. \quad (4)$$

¹Here we restrict to the isospin symmetry limit with $m_u = m_d = \hat{m}$.

Meson masses obviously satisfy the Gell-Mann-Oakes-Renner (4) and the Gell-Mann-Okubo relation $3M_\eta^2 + M_\pi^2 = 4M_K^2$. In the evaluation we use the following set of QCD parameters [19]:

$$\hat{m} = 7 \text{ MeV}, \quad \frac{m_s}{\hat{m}} = 25 \quad \text{and} \quad B = \frac{M_{\pi^+}^2}{2\hat{m}} = 1.4 \text{ GeV}. \quad (5)$$

Furthermore, the linearized effective Lagrangian fulfils the PCAC requirement [10], consistent with the Goldberger-Treiman relation (as shown later on).

To derive the properties of baryons, which are modelled as bound states of valence quarks surrounded by a meson cloud, we formulate perturbation theory. At zeroth order, the unperturbed Lagrangian simply describes the nucleon by three relativistic valence quarks which are confined by the effective one-body potential in the Dirac equation. The mass m_N^{core} of the three-quark core of the nucleon is then related to the single quark ground state energy \mathcal{E}_0 by $m_N^{core} = 3 \cdot \mathcal{E}_0$ (Here we do not discuss the removal of the spurious contribution to the baryon mass arising from the centre-of-mass motion of the bound state. It will be subject of a future publication.). For the unperturbed three-quark state we introduce the notation $|\phi_0\rangle$ with the normalization $\langle \phi_0 | \phi_0 \rangle = 1$. The single quark ground state energy \mathcal{E}_0 and wave function (w.f.) $u_0(\vec{x})$ are obtained from the Dirac equation

$$[-i\vec{\alpha}\vec{\nabla} + \beta S(r) + V(r) - \mathcal{E}_0]u_0(\vec{x}) = 0. \quad (6)$$

The quark w.f. $u_0(\vec{x})$ belongs to the basis of potential eigenstates (including excited quark and antiquark solutions) used for expanding the quark field operator $\psi(x)$. Here we restrict the expansion to the ground state contribution with

$$\psi(x) = b_0 u_0(\vec{x}) \exp(-i\mathcal{E}_0 t), \quad (7)$$

where b_0 is the corresponding single quark annihilation operator.

At the unperturbed level the current quark mass is not included in Eq. (6) to simplify our calculational technique. Instead we consider the quark mass term as a small perturbation [19], as will be discussed later on. Inclusion of a finite current quark mass leads to a displacement of the single quark energy which, for example, is relevant for the calculation of the sigma-term (see discussion in Ref. [10]); a quantity which vanishes in the chiral limit. On the other hand, the effect of a finite current quark mass on observables which survive in the chiral limit, like magnetic moments, charge radii, etc., is quite negligible.

For a given form of the potentials $S(r)$ and $V(r)$ the Dirac equation (6) can be solved numerically. Here, for the sake of simplicity, we use a variational *Gaussian ansatz* [20] for the quark wave function given by the analytical form:

$$u_0(\vec{x}) = N \exp\left[-\frac{\vec{x}^2}{2R^2}\right] \begin{pmatrix} 1 \\ i\rho \frac{\vec{\sigma}\vec{x}}{R} \end{pmatrix} \chi_s \chi_f \chi_c, \quad (8)$$

where

$$N = [\pi^{3/2} R^3 (1 + 3\rho^2/2)]^{-1/2} \quad (9)$$

is a constant fixed by the normalization condition

$$\int d^3x u_0^\dagger(x) u_0(x) \equiv 1; \quad (10)$$

χ_s, χ_f, χ_c are the spin, flavor and color quark wave functions, respectively. Our Gaussian ansatz contains two model parameters: the dimensional parameter R and the dimensionless parameter ρ . The parameter ρ can be related to the axial coupling constant g_A calculated in zeroth-order (or 3q-core) approximation:

$$g_A = \frac{5}{3} \left(1 - \frac{2\rho^2}{1 + \frac{3}{2}\rho^2} \right) = \frac{5}{3} \frac{1 + 2\gamma}{3}, \quad (11)$$

where γ is a relativistic reduction factor

$$\gamma = \frac{1 - \frac{3}{2}\rho^2}{1 + \frac{3}{2}\rho^2} = \frac{9}{10} g_A - \frac{1}{2}. \quad (12)$$

Note that since PCAC is fulfilled in our model [10], on the tree level the axial charge g_A is on the tree level related to the pion-nucleon coupling constant $G_{\pi NN}$ by the Goldberger-Treiman relation

$$G_{\pi NN} = \frac{5m_N}{3F} \left(1 - \frac{2\rho^2}{1 + \frac{3}{2}\rho^2} \right) \equiv \frac{m_N}{F} g_A. \quad (13)$$

where m_N is the physical nucleon mass.

The parameter R can be physically understood as the mean radius of the three-quark core and is related to the charge radius $\langle r_E^2 \rangle_{LO}^P$ of the proton in the leading-order (or zeroth-order) approximation as [10]

$$\langle r_E^2 \rangle_{LO}^P = \frac{3R^2}{2} \frac{1 + \frac{5}{2}\rho^2}{1 + \frac{3}{2}\rho^2} = R^2 \left(2 - \frac{\gamma}{2} \right). \quad (14)$$

In our calculations we use the value $g_A=1.25$ as obtained in ChPT [17]. We therefore have only one free parameter, R . In the numerical evaluation R is varied in the region from 0.55 fm to 0.65 fm corresponding to a change of $\langle r_E^2 \rangle_{LO}^P$ in the region from 0.5 fm² to 0.7 fm². The use of the Gaussian ansatz (8) in its exact form restricts the scalar confinement potential $S(r)$ to

$$S(r) = \underbrace{\frac{1 - 3\rho^2}{2\rho R}}_{=M} + \underbrace{\frac{\rho}{2R^3}}_{=c} r^2 = M + c r^2, \quad (15)$$

expressed in terms of the parameters R and ρ . The constant part of the scalar potential M can be interpreted as the constituent mass of the quark, which is simply a displacement of the current quark mass due to the potential $S(r)$. The parameter c is a constant defining the radial (quadratic) dependence of the scalar potential. Numerically, for our set of parameters, we get $M = 230 \pm 20$ MeV and $c = 0.007 \pm 0.002$ GeV³. Error bars for theoretical results quoted here and in the following correspond to the variation of the parameter R . For the vector potential we get the following expression

$$V(r) = \mathcal{E}_0 - \frac{1 + 3\rho^2}{2\rho R} + \frac{\rho}{2R^3} r^2, \quad (16)$$

where the single quark energy \mathcal{E}_0 is a free parameter in the Gaussian ansatz.

B. Perturbation theory and nucleon mass

Before setting out to present the renormalization scheme of the PCQM, we first define and discuss the quantities, relevant for mass and wave function renormalization. Following the Gell-Mann and Low theorem [21] we define the mass shift of the nucleonic three-quark ground state Δm_N due to the interaction with Goldstone mesons as²

$$\Delta m_N = {}^N \langle \phi_0 | \sum_{n=1}^{\infty} \frac{i^n}{n!} \int i\delta(t_1) d^4x_1 \dots d^4x_n T[\mathcal{L}_I(x_1) \dots \mathcal{L}_I(x_n)] | \phi_0 \rangle_c^N. \quad (17)$$

In Eq. (17) the strong interaction Lagrangian \mathcal{L}_I treated as a perturbation is defined as³

$$\mathcal{L}_I(x) = -\bar{\psi}(x) i\gamma^5 \frac{\hat{\Phi}(x)}{F} S(r)\psi(x) \quad (18)$$

and subscript "c" refers to contributions from connected graphs only. We evaluate Eq. (17) at one loop to order $o(1/F^2)$ using Wick's theorem and the appropriate propagators. For the quark field we use a Feynman propagator for a fermion in a binding potential. By restricting the summation over intermediate quark states to the ground state we get

$$iG_\psi(x, y) = \langle \phi_0 | T\{\psi(x)\bar{\psi}(y)\} | \phi_0 \rangle \rightarrow u_0(\vec{x})\bar{u}_0(\vec{y}) \exp[-i\mathcal{E}_0(x_0 - y_0)]\theta(x_0 - y_0). \quad (19)$$

For meson fields we use the free Feynman propagator for a boson field with

$$i\Delta_{ij}(x - y) = \langle 0 | T\{\Phi_i(x)\Phi_j(y)\} | 0 \rangle = \delta_{ij} \int \frac{d^4k}{(2\pi)^4} \frac{\exp[-ik(x - y)]}{M_\Phi^2 - k^2 - i\epsilon}. \quad (20)$$

Superscript "N" in Eq. (17) indicates that the matrix elements are projected on the respective nucleon states. The nucleon wave function $|N\rangle$ is conventionally set up by the product of the $SU(6)$ spin-flavor w.f. and $SU(3)_c$ color w.f. (see details in [23]), where the nonrelativistic single quark spin w.f. is replaced by the relativistic ground state solution of Eq. (8). Projection of "one-body" diagrams on the nucleon state refers to

$$\chi_{f'}^\dagger \chi_{s'}^\dagger I^{f'f} J^{s's} \chi_f \chi_s \xrightarrow{Proj.} \langle N | \sum_{i=1}^3 (I J)^{(i)} | N \rangle \quad (21)$$

where the single particle matrix element of the operators I and J , acting in flavor and spin space, is replaced by the one embedded in the nucleon state. For "two-body" diagrams with two independent quark indices i and j the projection prescription reads as

²We do not take into account the electromagnetic contribution to the nucleon mass since this effect is quite negligible.

³In the calculation of matrix elements we use the interaction Lagrangian and Wick's T -ordering product for field operators [22].

$$\chi_{f'}^\dagger \chi_{s'}^\dagger I_1^{f'f} J_1^{s's} \chi_f \chi_s \otimes \chi_{k'}^\dagger \chi_{\sigma'}^\dagger I_2^{k'k} J_2^{\sigma'\sigma} \chi_k \chi_\sigma \xrightarrow{Proj.} \langle N | \sum_{i \neq j}^3 (I_1 J_1)^{(i)} \otimes (I_2 J_2)^{(j)} | N \rangle. \quad (22)$$

The total nucleon mass is given by $m_N^r = m_N^{core} + \Delta m_N$. Superscript "r" refers to the renormalized value of the nucleon mass at one loop, that is the order of accuracy we are working in. The diagrams that contribute to the nucleon mass shift Δm_N at one loop are shown in Fig.1: meson cloud (Fig.1a) and meson exchange diagrams (Fig.1b). The explicit expression for the nucleon mass including one-loop corrections is given by

$$m_N^r = m_N^{core} + \Delta m_N = 3(\mathcal{E}_0 + \gamma \hat{m}) + \sum_{\Phi=\pi, K, \eta} d_N^\Phi \Pi(M_\Phi^2) \quad (23)$$

$$\text{with } d_N^\pi = \frac{171}{400}, \quad d_N^K = \frac{6}{19} d_N^\pi, \quad d_N^\eta = \frac{1}{57} d_N^\pi,$$

where d_N^Φ are the recoupling coefficients defining the partial contribution of the π , K and η -meson cloud to the mass shift of the nucleon. For the following it is also useful to separately indicate the contributions to d_N^Φ from the meson cloud ($d_N^{\Phi;MC}$) and the meson exchange diagrams ($d_N^{\Phi;EX}$):

$$\begin{aligned} d_N^{\pi;MC} &= \frac{81}{400}, & d_N^{K;MC} &\equiv d_N^K = \frac{54}{400}, & d_N^{\eta;MC} &= \frac{9}{400} \\ \text{and } d_N^{\pi;EX} &= \frac{90}{400}, & d_N^{K;EX} &= 0, & d_N^{\eta;EX} &= -\frac{6}{400}. \end{aligned} \quad (24)$$

The self-energy operators $\Pi(M_\Phi^2)$, corresponding to meson cloud contributions with definite flavor, differ only in their value for the meson mass and are given by

$$\Pi(M_\Phi^2) = - \left(\frac{g_A}{\pi F} \right)^2 \int_0^\infty \frac{dp p^4}{w_\Phi^2(p^2)} F_{\pi NN}^2(p^2). \quad (25)$$

For a meson with three-momentum \vec{p} the meson energy is $w_\Phi(p^2) = \sqrt{M_\Phi^2 + p^2}$ with $p = |\vec{p}|$ and $F_{\pi NN}(p^2)$ is the πNN form factor normalized to unity at zero recoil ($p^2 = 0$):

$$F_{\pi NN}(p^2) = \exp\left(-\frac{p^2 R^2}{4}\right) \left\{ 1 + \frac{p^2 R^2}{8} \left(1 - \frac{5}{3g_A} \right) \right\}. \quad (26)$$

Finally, the effect of a finite current quark mass \hat{m} on the nucleon mass shift is taken into account perturbatively (for details see [10]), resulting in the linear term $3\gamma\hat{m}$ in Eq. (23).

C. Renormalization of the PCQM

To redefine our perturbation series up to a given order in terms of renormalized quantities a set of counterterms $\delta\mathcal{L}$ has to be introduced in the Lagrangian. Thereby, the counterterms play a dual role: i) to maintain the proper definition of physical parameters, such as nucleon mass and, in particular, the nucleon charge and ii) to effectively reduce the number of Feynman diagrams to be evaluated.

1. Renormalization of the quark field

First, we introduce the renormalized quark field ψ^r with renormalized mass \mathcal{M}^r , substituting the original field ψ . Again, we restrict the expansion of the renormalized quark field to the ground state with

$$\psi_i^r(x; m_i^r) = b_0 u_0^r(\vec{x}; m_i^r) \exp(-i\mathcal{E}_0^r(m_i^r)t), \quad (27)$$

where "i" is the SU(3) flavor index; $\mathcal{E}_0^r(m_i^r)$ is the renormalized energy of the quark field in the ground state obtained from the solution of the Dirac equation

$$[-i\vec{\alpha}\vec{\nabla} + \beta m_i^r + \beta S(r) + V(r) - \mathcal{E}_0^r(m_i^r)]u_0^r(\vec{x}; m_i^r) = 0. \quad (28)$$

Using the derivations of the previous chapter, the renormalized mass m_i^r of the quark field is given by

$$\begin{aligned} m_u^r &= m_d^r = \hat{m}^r = \hat{m} - \delta\hat{m} = \hat{m} + \frac{1}{3\gamma} \sum_{\Phi=\pi,K,\eta} d_N^{\Phi;MC} \Pi(M_\Phi^2), \\ m_s^r &= m_s - \delta m_s = m_s + \frac{2}{3\gamma} \left[d_N^{K;MC} \Pi(M_K^2) + 2d_N^{\eta;MC} \Pi(M_\eta^2) \right], \end{aligned} \quad (29)$$

The meson exchange contribution will be included when introducing nucleon mass renormalization. For the quark masses we will use in the following the compact notation:

$$\mathcal{M}^r = \text{diag}\{\hat{m}^r, \hat{m}^r, m_s^r\} \quad \text{and} \quad \delta\mathcal{M} = \text{diag}\{\delta\hat{m}, \delta\hat{m}, \delta m_s\}. \quad (30)$$

The solutions of Eq. (28), $\mathcal{E}_0^r(m_i^r)$ and $u_0^r(\vec{x}; m_i^r)$, are functions of m_i^r . Obviously, the difference between nonstrange and strange quark solutions is solely due to the flavor dependent quark mass m_i^r . In the limit $m_i^r \rightarrow 0$ the solutions for nonstrange and strange quarks are degenerate: $\mathcal{E}_0^r(\hat{m}^r) \equiv \mathcal{E}_0$ and $u_0^r(\vec{x}; 0) \equiv u_0(\vec{x})$ (see Eq. (6)). For the renormalized wave function $u_0^r(\vec{x}; m_i^r)$ we again consider the Gaussian ansatz

$$u_0^r(\vec{x}; m_i^r) = N(m_i^r) \exp\left[-c(m_i^r) \frac{\vec{x}^2}{2R^2}\right] \left(\begin{array}{c} 1 \\ i\rho(m_i^r) \frac{\vec{\sigma}\vec{x}}{R} \end{array} \right) \chi_s \chi_f \chi_c \quad (31)$$

with normalization

$$\int d^3x u_0^{\dagger r}(x; m_i^r) u_0^r(x; m_i^r) \equiv 1. \quad (32)$$

In Eq. (31) the functions $N(m_i^r)$, $c(m_i^r)$ and $\rho(m_i^r)$ are normalized at the point $m_i^r = 0$ as follows:

$$N(0) = N, \quad c(0) = 1, \quad \rho(0) = \rho \quad (33)$$

The product $\rho(m_i^r)c(m_i^r)$ can be shown to be m_i^r -invariant and we therefore obtain the additional condition

$$\rho(m_i^r) c(m_i^r) \equiv \rho. \quad (34)$$

Treating m_i^r as a small perturbation, Eq. (28) can be solved perturbatively, resulting in:

$$\mathcal{E}_0^r(m_i^r) = \mathcal{E}_0 + \delta\mathcal{E}_0(m_i^r) \quad \text{and} \quad u_0^r(\vec{x}; m_i^r) = u_0(\vec{x}) + \delta u_0(\vec{x}; m_i^r) \quad (35)$$

where

$$\delta\mathcal{E}_0(m_i^r) = \gamma m_i^r \quad \text{and} \quad \delta u_0^r(\vec{x}; m_i^r) = \frac{m_i^r}{2} \frac{\rho R}{1 + \frac{3}{2}\rho^2} \left(\frac{1}{2} + \frac{21}{4}\rho^2 - \frac{\vec{x}^2}{R^2} + \gamma^0 \right) u_0(\vec{x}).$$

For our set of model parameters the ground state quark energy \mathcal{E}_0 is about 400 MeV and for the energy corrections $\delta\mathcal{E}_0$ relative to \mathcal{E}_0 we obtain

$$\left| \frac{\delta\mathcal{E}_0(\hat{m}^r)}{\mathcal{E}_0} \right| \approx 14\% \quad \text{and} \quad \left| \frac{\delta\mathcal{E}_0(m_s^r)}{\mathcal{E}_0} \right| \approx 18\%. \quad (36)$$

Given the small corrections expressed in Eq. (36), the perturbative treatment of a finite (renormalized) quark mass is a meaningful procedure.

2. Renormalized effective Lagrangian

Having set up renormalized fields and masses for the quarks we are in the position to rewrite the original Lagrangian. The renormalized effective Lagrangian including the photon field A_μ is now written as

$$\mathcal{L}_{full}^r = \mathcal{L}_\psi^r + \mathcal{L}_\Phi + \mathcal{L}_{ph} + \mathcal{L}_{int}^r. \quad (37)$$

The renormalized quark Lagrangian \mathcal{L}_ψ^r defines free nucleon dynamics at one-loop with

$$\begin{aligned} \mathcal{L}_\psi^r &= \mathcal{L}_{\bar{\psi}\psi}^r + \mathcal{L}_{(\bar{\psi}\psi)^2}^r, & \mathcal{L}_{\bar{\psi}\psi}^r &= \bar{\psi}^r(x) [i \not{\partial} - \mathcal{M}^r - S(r) - \gamma^0 V(r)] \psi^r(x) \\ \mathcal{L}_{(\bar{\psi}\psi)^2}^r &= c_\pi \sum_{i=1}^3 [\bar{\psi}^r(x) i\gamma^5 \lambda_i \psi^r(x)]^2 + c_K \sum_{i=4}^7 [\bar{\psi}^r(x) i\gamma^5 \lambda_i \psi^r(x)]^2 + c_\eta [\bar{\psi}^r(x) i\gamma^5 \lambda_8 \psi^r(x)]^2. \end{aligned} \quad (38)$$

The parameters $\delta\mathcal{M}$ of Eq. (30) guarantee the proper nucleon mass renormalization due to the meson cloud diagrams of Fig.1a. The terms contained in $\mathcal{L}_{(\bar{\psi}\psi)^2}^r$ are introduced for the purpose of nucleon mass renormalization due to the meson exchange diagram of Fig.1b. The corresponding renormalization parameters c_π , c_K and c_η are deduced from Eqs. (23) and (24) as

$$c_\Phi = -\frac{9}{200} \frac{(2\pi R^2)^{3/2}}{(1 - \gamma^2)} \Pi(M_\Phi^2). \quad (39)$$

The free meson Lagrangian \mathcal{L}_Φ is written as

$$\mathcal{L}_\Phi = -\frac{1}{2} \sum_{i,j=1}^8 \Phi_i(x) (\delta_{ij} \square + M_{ij}^2) \Phi_j(x) \quad (40)$$

where $\square = \partial^\mu \partial_\mu$ and M_{ij}^2 is the diagonal meson mass matrix with

$$M_{11}^2 = M_{22}^2 = M_{33}^2 = M_\pi^2, \quad M_{44}^2 = M_{55}^2 = M_{66}^2 = M_{77}^2 = M_K^2, \quad M_{88}^2 = M_\eta^2. \quad (41)$$

For the photon field A_μ we have the usual kinetic term

$$\mathcal{L}_{ph} = -\frac{1}{4}F_{\mu\nu}(x)F^{\mu\nu}(x) \quad \text{with} \quad F_{\mu\nu}(x) = \partial_\nu A_\mu(x) - \partial_\mu A_\nu(x). \quad (42)$$

The renormalized interaction Lagrangian $\mathcal{L}_{int}^r = \mathcal{L}_{str}^r + \mathcal{L}_{em}^r$ contains a part due to the strong

$$\mathcal{L}_{str}^r = \mathcal{L}_I^{str} + \delta\mathcal{L}^{str} \quad (43)$$

and the electromagnetic interaction

$$\mathcal{L}_{em}^r = \mathcal{L}_I^{em} + \delta\mathcal{L}^{em}. \quad (44)$$

The strong interaction term \mathcal{L}_I^{str} is given by

$$\mathcal{L}_I^{str} = -\bar{\psi}^r(x)i\gamma^5\frac{\hat{\Phi}(x)}{F}S(r)\psi^r(x) \quad (45)$$

The interaction of mesons and quarks with the electromagnetic field is described by

$$\begin{aligned} \mathcal{L}_I^{em} = & -eA_\mu(x)\bar{\psi}^r(x)\gamma^\mu Q\psi^r(x) - eA_\mu(x)\sum_{i,j=1}^8\left[f_{3ij} + \frac{f_{8ij}}{\sqrt{3}}\right]\Phi_i(x)\partial^\mu\Phi_j(x) \\ & + \frac{e^2}{2}A_\mu^2(x)\sum_{i=1,2,4,5}\Phi_i^2(x). \end{aligned} \quad (46)$$

The term \mathcal{L}_I^{em} is generated by minimal substitution with

$$\begin{aligned} \partial_\mu\psi^r & \rightarrow D_\mu\psi^r = \partial_\mu\psi^r + ieQA_\mu\psi^r, \\ \partial_\mu\Phi_i & \rightarrow D_\mu\Phi_i = \partial_\mu\Phi_i + e\left[f_{3ij} + \frac{f_{8ij}}{\sqrt{3}}\right]A_\mu\Phi_j \end{aligned} \quad (47)$$

where Q is the quark charge matrix and f_{ijk} are the totally antisymmetric structure constants of $SU(3)$.

The set of counterterms, denoted by $\delta\mathcal{L}^{str}$ and $\delta\mathcal{L}^{em}$, is explicitly given by

$$\delta\mathcal{L}^{str} = \delta\mathcal{L}_1^{str} + \delta\mathcal{L}_2^{str} + \delta\mathcal{L}_3^{str},$$

with

$$\delta\mathcal{L}_1^{str} = \bar{\psi}^r(x)(Z-1)[i\cancel{\partial} - \mathcal{M}^r - S(r) - \gamma^0V(r)]\psi^r(x),$$

$$\delta\mathcal{L}_2^{str} = -\bar{\psi}^r(x)\delta\mathcal{M}\psi^r(x),$$

$$\delta\mathcal{L}_3^{str} = -c_\pi\sum_{i=1}^3[\bar{\psi}^r(x)i\gamma^5\lambda_i\psi^r(x)]^2 - c_K\sum_{i=4}^7[\bar{\psi}^r(x)i\gamma^5\lambda_i\psi^r(x)]^2 - c_\eta[\bar{\psi}^r(x)i\gamma^5\lambda_8\psi^r(x)]^2,$$

and

$$\delta\mathcal{L}^{em} = -eA_\mu(x)\bar{\psi}^r(x)(Z-1)\gamma^\mu Q\psi^r(x).$$

Here, $Z = \text{diag}\{\hat{Z}, \hat{Z}, Z_s\}$ is the diagonal matrix of renormalization constants (\hat{Z} for u, d -quarks and Z_s for s -quark). The values of \hat{Z} and Z_s are determined by the charge conservation condition. The simplest way to fix \hat{Z} and Z_s is on the quark level. The same set of values for \hat{Z} and Z_s is also obtained when requiring charge conservation on the baryon level. Results for \hat{Z} and Z_s will be discussed below.

Now we briefly explain the role of each counterterm and why the set of constants \hat{Z} and Z_s is identical in $\delta\mathcal{L}_1^{str}$ and $\delta\mathcal{L}^{em}$. The counterterm $\delta\mathcal{L}^{em}$ is introduced to guarantee charge conservation. The counterterm $\delta\mathcal{L}_1^{str}$, containing the same renormalization constants \hat{Z} and Z_s as in $\delta\mathcal{L}^{em}$, is added to fulfil electromagnetic local gauge invariance on the Lagrangian level. The same term also leads to conservation of the vector current (baryon number conservation). Alternatively, $\delta\mathcal{L}^{em}$ can also be deduced from $\delta\mathcal{L}_1^{str}$ by minimal substitution. In covariant theories the equality of the renormalization constants in $\delta\mathcal{L}_1^{str}$ and $\delta\mathcal{L}^{em}$ is known as the Ward identity. The counterterms $\delta\mathcal{L}_2^{str}$ and $\delta\mathcal{L}_3^{str}$ compensate the contributions of the meson cloud (Fig.1a) and meson exchange diagrams (Fig.1b) to the nucleon mass m_N^r (The contribution of meson cloud and exchange diagrams is already taken into account in the renormalized quark Lagrangian \mathcal{L}_ψ^r).

3. Renormalization of nucleon mass and charge

Now we illustrate the explicit role of the counterterms when performing the calculation of the nucleon mass and the nucleon charge. The renormalized nucleon mass m_N^r is defined by the expectation value of the Hamiltonian \mathcal{H}_ψ^r (as derived from the Lagrangian \mathcal{L}_ψ^r) averaged over state $|\phi_0\rangle$ and projected on the respective nucleon states:

$$m_N^r \equiv {}^N\langle\phi_0|\int\delta(t)d^4x\mathcal{H}_\psi^r(x)|\phi_0\rangle^N, \quad (48)$$

By inclusion of the counterterms the strong interaction Lagrangian \mathcal{L}_r^{str} should give a zero contribution to the shift of the renormalized nucleon mass at one loop, that is

$$\begin{aligned} \Delta m_N^r &= {}^N\langle\phi_0|\sum_{n=1}^2\frac{i^n}{n!}\int i\delta(t_1)d^4x_1\dots d^4x_n T[\mathcal{L}_r^{str}(x_1)\dots\mathcal{L}_r^{str}(x_n)]|\phi_0\rangle_c^N \\ &= {}^N\langle\phi_0|-\frac{i}{2}\int\delta(t_1)d^4x_1d^4x_2 T[\mathcal{L}_I^{str}(x_1)\mathcal{L}_I^{str}(x_2)]|\phi_0\rangle_c^N \\ &\quad - {}^N\langle\phi_0|\int\delta(t)d^4x\sum_{i=1}^3\delta\mathcal{L}_i^{str}(x)|\phi_0\rangle^N\equiv 0. \end{aligned} \quad (49)$$

The propagator of the renormalized quark field ψ^r is given by

$$iG_{\psi^r}(x, y) = \langle\phi_0|T\{\psi^r(x)\bar{\psi}^r(y)\}|\phi_0\rangle \rightarrow u_0^r(\vec{x})\bar{u}_0^r(\vec{y})\exp[-i\mathcal{E}_0^r(x_0 - y_0)]\theta(x_0 - y_0). \quad (50)$$

It differs from the unperturbed quark propagator $iG_\psi(x, y)$ by terms of order \hat{m}^r , which in turn only contribute to the two-loop calculations. Thus, to the order of accuracy we are working in (up to one-loop perturbation theory) it is sufficient to use the unperturbed quark propagator $iG_\psi(x, y)$ instead of the renormalized one.

To prove Eq. (49), we first note that the contribution of the counterterm $\delta\mathcal{L}_1^{str}$ is equal to zero due to the equation of motion (28), that is

$${}^N\langle \phi_0 | \int \delta(t) d^4x \delta \mathcal{L}_1^{str}(x) | \phi_0 \rangle^N \equiv 0. \quad (51)$$

The counterterms $\delta \mathcal{L}_2^{str}$ and $\delta \mathcal{L}_3^{str}$ compensate the contribution of the meson cloud (Fig.1a) and exchange diagrams (Fig.1b), respectively, with

$$\begin{aligned} & {}^N\langle \phi_0 | -\frac{i}{2} \int \delta(t_1) d^4x_1 d^4x_2 T[\mathcal{L}_I^{str}(x_1) \mathcal{L}_I^{str}(x_2)] | \phi_0 \rangle_c^N \\ & - {}^N\langle \phi_0 | \int \delta(t) d^4x [\delta \mathcal{L}_2^{str}(x) + \delta \mathcal{L}_3^{str}(x)] | \phi_0 \rangle^N \equiv 0, \end{aligned} \quad (52)$$

hence Eq. (49) is fulfilled. The calculation of the nucleon mass m_N^r at one-loop can then either be done with the "unrenormalized" Lagrangian \mathcal{L}_{eff} or with the "renormalized" version \mathcal{L}_{full}^r (37). Both results for m_N^r are identical and are given by Eq. (23).

Now we consider the nucleon charge and prove that the properly introduced counterterms guarantee charge conservation. Using Noether's theorem we first derive from the renormalized Lagrangian (37) the electromagnetic, renormalized current operator:

$$j_r^\mu = j_{\psi^r}^\mu + j_\Phi^\mu + \delta j_{\psi^r}^\mu. \quad (53)$$

It contains the quark component $j_{\psi^r}^\mu$, the charged meson component j_Φ^μ and the contribution of the counterterm $\delta j_{\psi^r}^\mu$:

$$j_{\psi^r}^\mu = \bar{\psi}^r \gamma^\mu Q \psi^r \equiv \frac{1}{3} [2 \bar{u}^r \gamma^\mu u^r - \bar{d}^r \gamma^\mu d^r - \bar{s}^r \gamma^\mu s^r], \quad (54)$$

$$j_\Phi^\mu = \left[f_{3ij} + \frac{f_{8ij}}{\sqrt{3}} \right] \Phi_i \partial^\mu \Phi_j \equiv [\pi^- i \partial^\mu \pi^+ - \pi^+ i \partial^\mu \pi^- + K^- i \partial^\mu K^+ - K^+ i \partial^\mu K^-],$$

and

$$\delta j_{\psi^r}^\mu = \bar{\psi}^r (Z - 1) \gamma^\mu Q \psi^r \equiv \frac{1}{3} [2 (\hat{Z} - 1) \bar{u}^r \gamma^\mu u^r - (\hat{Z} - 1) \bar{d}^r \gamma^\mu d^r - (Z_s - 1) \bar{s}^r \gamma^\mu s^r].$$

The renormalized nucleon charge Q_N^r at one loop is defined as

$$Q_N^r = {}^N\langle \phi_0 | \sum_{n=0}^2 \frac{i^n}{n!} \int \delta(t) d^4x d^4x_1 \dots d^4x_n T[\mathcal{L}_r^{str}(x_1) \dots \mathcal{L}_r^{str}(x_n) j_r^0(x)] | \phi_0 \rangle_c^N. \quad (55)$$

Charge conservation requires that the nucleon charge is not changed after renormalization, that is

$$Q_N^r \equiv Q_N = \begin{cases} 1 & \text{for } N = p \quad (\text{proton}) \\ 0 & \text{for } N = n \quad (\text{neutron}). \end{cases} \quad (56)$$

Thereby, Q_N is the nucleon charge in the three-quark core approximation, which is defined as the expectation value of the quark charge operator $\hat{Q}_\psi = \int d^3x j_\psi^0(x)$ taken between the unperturbed 3q-states $|\phi_0\rangle$:

$$Q_N = {}^N\langle \phi_0 | \int \delta(t) d^4x j_\psi^0(x) | \phi_0 \rangle^N. \quad (57)$$

Eqs. (55)-(57) completely define *the charge conservation condition* within our approach.

From nucleon charge conservation at one loop we obtain a condition on the renormalization constant \hat{Z} . To fix the constant Z_s we should consider the charge conservation of baryons containing s -quarks, e.g. Σ^+ - baryon. In the one-loop approximation following diagrams contribute to the nucleon charge Q_N^r (see Figs.2a-l): three-quark diagram (Fig.2a) with insertion of the quark current $j_{\psi^r}^\mu$, three-quark diagram (Fig.2b) with the counterterm $\delta j_{\psi^r}^\mu$ (three-quark counterterm diagram), meson-cloud diagram (Fig.2c) with the meson current j_Φ^μ , vertex correction diagram (Fig.2d) with the quark current $j_{\psi^r}^\mu$, self-energy diagrams (Figs.2e and 2f) and exchange current diagrams (Figs.2i and 2j) with insertion of the quark current $j_{\psi^r}^\mu$. We also obtain a set of diagrams (Figs.2g, 2h, 2k and 2l) generated by the counterterms $\delta\mathcal{L}_2^{str}(x)$ and $\delta\mathcal{L}_3^{str}(x)$. The contribution of the counterterm $\delta\mathcal{L}_1^{str}(x)$ is equal to zero due to the equation of motion (28). By definition of the counterterms $\delta\mathcal{L}_2^{str}(x)$ and $\delta\mathcal{L}_3^{str}(x)$, the self-energy and the meson exchange current diagrams of Fig.2e, f, i, j are compensated by the counterterm diagrams of Fig.2g, h, k and l, respectively.

The contribution of the three-quark diagram (Fig.2a) to the nucleon charge is trivially given by

$$Q_N^{r;a} = {}^N\langle\phi_0|\int\delta(t)d^4xj_{\psi^r}^0(x)|\phi_0\rangle^N\equiv Q_N. \quad (58)$$

The three-quark counterterm diagram (Fig.2b) is simply related to the one of Fig.2a with:

$$Q_N^{r;b} = (\hat{Z} - 1)Q_N^{r;a} = (\hat{Z} - 1){}^N\langle\phi_0|\int\delta(t)d^4xj_{\psi^r}^0(x)|\phi_0\rangle^N\equiv (\hat{Z} - 1)Q_N. \quad (59)$$

The meson cloud diagram (Fig.2c) generates the term

$$Q_N^{r;c} = \frac{27}{400}\left(\frac{g_A}{\pi F}\right)^2\int_0^\infty dp p^4 F_{\pi NN}^2(p^2)\sum_{\Phi=\pi,K}\frac{q_N^{\Phi;c}}{w_\Phi^3(p^2)} \quad (60)$$

where

$$q_N^{\pi;c} = \begin{cases} \frac{2}{3} & \text{for } N = p \\ -\frac{2}{3} & \text{for } N = n \end{cases}, \quad q_N^{K;c} = \begin{cases} \frac{4}{3} & \text{for } N = p \\ \frac{2}{3} & \text{for } N = n \end{cases}.$$

The contribution of the vertex correction diagram (Fig.2d) is given by

$$Q_N^{r;d} = \frac{27}{400}\left(\frac{g_A}{\pi F}\right)^2\int_0^\infty dp p^4 F_{\pi NN}^2(p^2)\sum_{\Phi=\pi,K,\eta}\frac{q_N^{\Phi;d}}{w_\Phi^3(p^2)} \quad (61)$$

where

$$q_N^{\pi;d} = \begin{cases} \frac{1}{3} & \text{for } N = p \\ \frac{2}{3} & \text{for } N = n \end{cases}, \quad q_N^{K;d} = \begin{cases} -\frac{2}{3} & \text{for } N = p \\ -\frac{2}{3} & \text{for } N = n \end{cases}, \quad q_N^{\eta;d} = \begin{cases} \frac{1}{9} & \text{for } N = p \\ 0 & \text{for } N = n \end{cases}.$$

To guarantee charge conservation, the sum of meson-cloud and vertex correction diagrams must be compensated by the counterterm contribution:

$$Q_N^{r;b} + Q_N^{r;c} + Q_N^{r;d} \equiv 0. \quad (62)$$

The last requirement fixes the value of the renormalization constant \hat{Z} at one loop to

$$\hat{Z} = 1 - \frac{27}{400} \left(\frac{g_A}{\pi F} \right)^2 \int_0^\infty dp p^4 F_{\pi NN}^2(p^2) \left\{ \frac{1}{w_\pi^3(p^2)} + \frac{2}{3w_K^3(p^2)} + \frac{1}{9w_\eta^3(p^2)} \right\}. \quad (63)$$

In the two-flavor picture, that is when we restrict to the pion cloud contribution only, we obtain a value of $\hat{Z} = 0.9 \pm 0.02$ for our set of parameters. The contribution of kaon and η -meson loops to the constant \hat{Z} is strongly suppressed due to the energy denominators in Eq. (63). In the three-flavor picture we get $\hat{Z} = 0.88 \pm 0.03$, which deviates only slightly from the two-flavor result. The minor role of kaon and η -meson loop contributions to nucleon properties was also found in our previous analysis of meson-nucleon sigma-terms [10]. As already mentioned, the renormalization constant Z_s is fixed from the charge conservation of baryons containing strange quarks (e.g. Σ^+ -baryon). Here we obtain the analytical result:

$$Z_s = 1 - \frac{27}{400} \left(\frac{g_A}{\pi F} \right)^2 \int_0^\infty dp p^4 F_{\pi NN}^2(p^2) \left\{ \frac{4}{3w_K^3(p^2)} + \frac{4}{9w_\eta^3(p^2)} \right\}. \quad (64)$$

In the $SU(3)$ flavor symmetry limit ($m_u = m_d = m_s$) both renormalization constants \hat{Z} and Z_s are degenerate. Again, charge conservation within our approach is fulfilled both on the quark level (when we directly calculate the charge of u , d or s -quark at one loop) and on the baryon level. With the value of \hat{Z} being close to unity for our set of parameters the perturbative treatment of the meson cloud is also justified.

III. ELECTROMAGNETIC FORM FACTORS OF THE NUCLEON

It is well-known that noncovariant hadron models should explicitly address the question of local gauge invariance of electromagnetic form factors (for a detailed discussion see Refs. [24]- [28]). Particularly, even when starting from a gauge-invariant Lagrangian the resulting physical amplitudes are not necessarily gauge invariant in an arbitrary frame due to the use of noncovariant techniques (e.g. noncovariant particle propagators). The lack of Lorentz covariance in our approach is linked to the static potential solutions for the quark fields and, as consequence, to the use of a noncovariant quark propagator. However, when restricting our kinematics to a specific frame, that is the Breit frame, gauge invariance is fulfilled due to the decoupling of the time and vector components of the electromagnetic current operator.

Next we follow the original work by Sachs et al. [24,25] and Thomas et al. [4,26,27] to set up the formalism for the electromagnetic form factors of the nucleon. In the Breit frame the initial momentum of the nucleon is $p = (E, -\vec{q}/2)$, the final momentum is $p' = (E, \vec{q}/2)$ and the 4-momentum of the photon is $q = (0, \vec{q})$ with $p' = p + q$. With the space-like momentum transfer squared given as $Q^2 = -q^2 = \vec{q}^2$, in the Breit frame the nucleon charge G_E^N and magnetic G_M^N (Sachs) form factors are defined by [27]

$$\begin{aligned} \langle N_{s'} \left(\frac{\vec{q}}{2} \right) | J^0(0) | N_s \left(-\frac{\vec{q}}{2} \right) \rangle &= \chi_{N_{s'}}^\dagger \chi_{N_s} G_E^N(Q^2), \\ \langle N_{s'} \left(\frac{\vec{q}}{2} \right) | \vec{J}(0) | N_s \left(-\frac{\vec{q}}{2} \right) \rangle &= \chi_{N_{s'}}^\dagger \frac{i\vec{\sigma}_N \times \vec{q}}{2m_N} \chi_{N_s} G_M^N(Q^2). \end{aligned} \quad (65)$$

Here, $J^0(0)$ and $\vec{J}(0)$ are the time and space component of the electromagnetic current operator (53); χ_{N_s} and $\chi_{N_{s'}}^\dagger$ are the nucleon spin w.f. in the initial and final state; $\vec{\sigma}_N$ is the nucleon spin matrix. Electromagnetic gauge invariance on the baryon level is fulfilled in the Breit frame. In particular, for on-mass shell nucleons we verify the Ward-Takahashi identity without referring to the explicit form of the nucleon charge and magnetic form factors:

$$\begin{aligned} q_\mu < N_{s'} \left(\frac{\vec{q}}{2} \right) | j_r^\mu(0) | N_s \left(-\frac{\vec{q}}{2} \right) > &= \underbrace{q_0}_{\equiv 0} \cdot < N_{s'} \left(\frac{\vec{q}}{2} \right) | j_r^0(0) | N_s \left(-\frac{\vec{q}}{2} \right) > \\ + \vec{q} \cdot < N_{s'} \left(\frac{\vec{q}}{2} \right) | \vec{j}_r(0) | N_s \left(-\frac{\vec{q}}{2} \right) > &= \chi_{N_{s'}}^\dagger \vec{q} \cdot \frac{i\vec{\sigma}_N \times \vec{q}}{2m_N} \chi_{N_s} G_M^N(Q^2) \equiv 0 \end{aligned} \quad (66)$$

At zero recoil ($q^2 = 0$) the Sachs form factors satisfy the following normalization conditions

$$G_E^p(0) = 1, \quad G_E^n(0) = 0, \quad G_M^p(0) = \mu_p, \quad G_M^n(0) = \mu_n, \quad (67)$$

where μ_p and μ_n are the magnetic moments of the proton and the neutron, respectively.

The charge radii of the nucleons are given by

$$\begin{aligned} \langle r^2 \rangle_E^p &= -6 \frac{dG_E^p(Q^2)}{dQ^2} \Big|_{Q^2=0}, & \langle r^2 \rangle_E^n &= -6 \frac{dG_E^n(Q^2)}{dQ^2} \Big|_{Q^2=0}, \\ \langle r^2 \rangle_M^N &= -\frac{6}{G_M^N(0)} \frac{dG_M^N(Q^2)}{dQ^2} \Big|_{Q^2=0}. \end{aligned} \quad (68)$$

In the PCQM the charge and magnetic form factors of nucleon are defined by

$$\begin{aligned} \chi_{N_{s'}}^\dagger \chi_{N_s} G_E^N(Q^2) &= {}^N \langle \phi_0 | \sum_{n=0}^2 \frac{i^n}{n!} \int \delta(t) d^4x d^4x_1 \dots d^4x_n e^{-iqx} \\ &\quad \times T[\mathcal{L}_r^{str}(x_1) \dots \mathcal{L}_r^{str}(x_n) j_r^0(x)] | \phi_0 \rangle_c^N, \\ \chi_{N_{s'}}^\dagger \frac{i\vec{\sigma}_N \times \vec{q}}{2m_N} \chi_{N_s} G_M^N(Q^2) &= {}^N \langle \phi_0 | \sum_{n=0}^2 \frac{i^n}{n!} \int \delta(t) d^4x d^4x_1 \dots d^4x_n e^{-iqx} \\ &\quad \times T[\mathcal{L}_r^{str}(x_1) \dots \mathcal{L}_r^{str}(x_n) \vec{j}_r(x)] | \phi_0 \rangle_c^N. \end{aligned} \quad (69)$$

The diagrams of Figs.2a-d contribute to the charge form factor of the nucleon. For the magnetic form factors we have to include an additional term due to the "meson-in-flight" diagram indicated in Fig.3. The other possible diagrams at one-loop (like self-energy current and meson-exchange current diagrams of Fig.2) are compensated by the counterterms (see previous discussion about renormalization of the nucleon charge).

In the following we indicate the analytical expressions for the relevant diagrams:

a) Tree-quark diagram (3q) (Fig.2a):

$$\begin{aligned} G_E^p(Q^2) \Big|_{3q} &= G_E^p(Q^2) \Big|_{3q}^{LO} + G_E^p(Q^2) \Big|_{3q}^{NLO}, & G_E^n(Q^2) \Big|_{3q} &\equiv 0, \\ G_M^p(Q^2) \Big|_{3q} &= G_M^p(Q^2) \Big|_{3q}^{LO} + G_M^p(Q^2) \Big|_{3q}^{NLO}, & G_M^n(Q^2) \Big|_{3q} &\equiv -\frac{2}{3} G_M^p(Q^2) \Big|_{3q}, \end{aligned} \quad (70)$$

where $G_{E,M}^N(Q^2)\Big|_{3q}^{LO}$ are the leading-order (LO) terms of the tree-quark diagram evaluated with the unperturbed quark w.f. $u_0(\vec{x})$; $G_E^p(Q^2)\Big|_{3q}^{NLO}$ is a correction due to the modification of the quark w.f. $u_0(\vec{x}) \rightarrow u_0^r(\vec{x}; \hat{m}^r)$ referred to as next-to-leading order (NLO):

$$\begin{aligned}
G_E^p(Q^2)\Big|_{3q}^{LO} &= \exp\left(-\frac{Q^2 R^2}{4}\right) \left(1 - \frac{\rho^2}{1 + \frac{3}{2}\rho^2} \frac{Q^2 R^2}{4}\right), \\
G_E^p(Q^2)\Big|_{3q}^{NLO} &= \exp\left(-\frac{Q^2 R^2}{4}\right) \hat{m}^r \frac{Q^2 R^3 \rho}{4(1 + \frac{3}{2}\rho^2)^2} \left(\frac{1 + 7\rho^2 + \frac{15}{4}\rho^4}{1 + \frac{3}{2}\rho^2} - \frac{Q^2 R^2}{4} \rho^2\right), \\
G_M^p(Q^2)\Big|_{3q}^{LO} &= \exp\left(-\frac{Q^2 R^2}{4}\right) \frac{2m_N \rho R}{1 + \frac{3}{2}\rho^2}, \\
G_M^p(Q^2)\Big|_{3q}^{NLO} &= G_M^p(Q^2)\Big|_{3q}^{LO} \cdot \hat{m}^r \frac{R\rho}{1 + \frac{3}{2}\rho^2} \left(\frac{Q^2 R^2}{4} - \frac{2 - \frac{3}{2}\rho^2}{1 + \frac{3}{2}\rho^2}\right).
\end{aligned} \tag{71}$$

b) Three-quark counterterm (CT) (Fig.2b):

$$\begin{aligned}
G_E^p(Q^2)\Big|_{CT} &\equiv (\hat{Z} - 1) G_E^p(Q^2)\Big|_{3q}^{LO}, & G_E^m(Q^2)\Big|_{CT} &\equiv 0, \\
G_M^p(Q^2)\Big|_{CT} &\equiv (\hat{Z} - 1) G_M^p(Q^2)\Big|_{3q}^{LO}, & G_M^m(Q^2)\Big|_{CT} &\equiv -\frac{2}{3} G_M^p(Q^2)\Big|_{CT}.
\end{aligned} \tag{72}$$

c) Meson-cloud diagram (MC) (Fig.2c):

$$\begin{aligned}
G_E^N(Q^2)\Big|_{MC} &= \frac{9}{400} \left(\frac{g_A}{\pi F}\right)^2 \int_0^\infty dp p^2 \int_{-1}^1 dx (p^2 + p\sqrt{Q^2}x) \mathcal{F}_{\pi NN}(p^2, Q^2, x) t_E^N(p^2, Q^2, x)\Big|_{MC} \\
G_M^N(Q^2)\Big|_{MC} &= \frac{3}{40} m_N \left(\frac{g_A}{\pi F}\right)^2 \int_0^\infty dp p^4 \int_{-1}^1 dx (1 - x^2) \mathcal{F}_{\pi NN}(p^2, Q^2, x) t_M^N(p^2, Q^2, x)\Big|_{MC}
\end{aligned} \tag{73}$$

where

$$\begin{aligned}
\mathcal{F}_{\pi NN}(p^2, Q^2, x) &= F_{\pi NN}(p^2) F_{\pi NN}(p^2 + Q^2 + 2p\sqrt{Q^2}x), \\
t_E^p(p^2, Q^2, x)\Big|_{MC} &= C_\pi^{11}(p^2, Q^2, x) + 2C_K^{11}(p^2, Q^2, x), \\
t_E^n(p^2, Q^2, x)\Big|_{MC} &= -C_\pi^{11}(p^2, Q^2, x) + C_K^{11}(p^2, Q^2, x), \\
t_M^p(p^2, Q^2, x)\Big|_{MC} &= D_\pi^{22}(p^2, Q^2, x) + \frac{4}{5} D_K^{22}(p^2, Q^2, x), \\
t_M^n(p^2, Q^2, x)\Big|_{MC} &= -D_\pi^{22}(p^2, Q^2, x) - \frac{1}{5} D_K^{22}(p^2, Q^2, x), \\
D_\Phi^{n_1 n_2}(p^2, Q^2, x) &= \frac{1}{w_\Phi^{n_1}(p^2) w_\Phi^{n_2}(p^2 + Q^2 + 2p\sqrt{Q^2}x)}, \\
C_\Phi^{n_1 n_2}(p^2, Q^2, x) &= \frac{2D_\Phi^{n_1 n_2}(p^2, Q^2, x)}{w_\Phi(p^2) + w_\Phi(p^2 + Q^2 + 2p\sqrt{Q^2}x)}.
\end{aligned}$$

d) Vertex-correction diagram (VC) (Fig.2d):

$$G_{E(M)}^N(Q^2)\Big|_{VC} = G_{E(M)}^p(Q^2)\Big|_{3q}^{LO} \cdot \frac{9}{200} \left(\frac{g_A}{\pi F}\right)^2 \int_0^\infty dp p^4 F_{\pi NN}^2(p^2) t_{E(M)}^N(p^2)\Big|_{VC}, \quad (74)$$

where

$$\begin{aligned} t_E^p(p^2)\Big|_{VC} &= \frac{1}{2}W_\pi(p^2) - W_K(p^2) + \frac{1}{6}W_\eta(p^2), \\ t_E^n(p^2)\Big|_{VC} &= W_\pi(p^2) - W_K(p^2), \\ t_M^p(p^2)\Big|_{VC} &= \frac{1}{18}W_\pi(p^2) + \frac{1}{9}W_K(p^2) - \frac{1}{18}W_\eta(p^2), \\ t_M^n(p^2)\Big|_{VC} &= -\frac{2}{9}W_\pi(p^2) + \frac{1}{9}W_K(p^2) + \frac{1}{27}W_\eta(p^2), \\ W_\Phi(p^2) &= \frac{1}{w_\Phi^3(p^2)}. \end{aligned}$$

e) Meson-in-flight diagram (MF) (Fig.3):

$$\begin{aligned} G_E^p(Q^2)\Big|_{MF} &\equiv 0, \quad G_E^n(Q^2)\Big|_{MF} \equiv 0, \quad G_M^n(Q^2)\Big|_{MF} \equiv -G_M^p(Q^2)\Big|_{MF} \quad (75) \\ G_M^p(Q^2)\Big|_{MF} &= \frac{9}{100} m_N \left(\frac{g_A}{\pi F}\right)^2 \int_0^\infty dp p^4 \int_{-1}^1 dx (1-x^2) \mathcal{F}_{\pi NN}(p^2, Q^2, x) D_\pi^{22}(p^2, Q^2, x). \end{aligned}$$

We do not include the modification of the quark w.f. in the calculation of one-loop diagrams (Figs.2b, 2c, 2d and 3) since it only gives corrections to the next (two-loop) order in perturbation theory.

We start our analysis with the magnetic moments of nucleons, μ_p and μ_n , given by the expressions (in units of nucleon magnetons)

$$\begin{aligned} \mu_p &= \mu_p^{LO} \left[1 + \delta - \frac{1}{400} \left(\frac{g_A}{\pi F}\right)^2 \int_0^\infty dp p^4 F_{\pi NN}^2(p^2) \left\{ \frac{26}{w_\pi^3(p^2)} + \frac{16}{w_K^3(p^2)} + \frac{4}{w_\eta^3(p^2)} \right\} \right] \quad (76) \\ &\quad + \frac{m_N}{50} \left(\frac{g_A}{\pi F}\right)^2 \int_0^\infty dp p^4 F_{\pi NN}^2(p^2) \left\{ \frac{11}{w_\pi^4(p^2)} + \frac{4}{w_K^4(p^2)} \right\} \\ \mu_n &= -\frac{2}{3} \mu_p^{LO} \left[1 + \delta - \frac{1}{400} \left(\frac{g_A}{\pi F}\right)^2 \int_0^\infty dp p^4 F_{\pi NN}^2(p^2) \left\{ \frac{21}{w_\pi^3(p^2)} + \frac{21}{w_K^3(p^2)} + \frac{4}{w_\eta^3(p^2)} \right\} \right] \\ &\quad - \frac{m_N}{50} \left(\frac{g_A}{\pi F}\right)^2 \int_0^\infty dp p^4 F_{\pi NN}^2(p^2) \left\{ \frac{11}{w_\pi^4(p^2)} + \frac{1}{w_K^4(p^2)} \right\} \end{aligned}$$

where

$$\mu_p^{LO} = G_M^p(0)\Big|_{3q}^{LO} = \frac{2m_N \rho R}{1 + \frac{3}{2}\rho^2}$$

is the leading-order contribution to the proton magnetic moment. The factor

$$\delta = -\hat{m}^r R \rho \frac{2 - \frac{3}{2}\rho^2}{(1 + \frac{3}{2}\rho^2)^2} \quad (77)$$

defines the NLO correction to the nucleon magnetic moments due to the modification of the quark w.f. (see Eq. (71)). Note that the well-known SU_6 relation between nucleon magnetic moments $\mu_n/\mu_p = -2/3$ can be easily deduced from Eq. (76) if: i) we restrict to contributions from one-body diagrams in Figs.2a-d, corresponding to the additive quark picture, and ii) apply the $SU(3)$ -flavor limit ($M_\pi = M_K = M_\eta = M_\Phi$). In particular, we have

$$\begin{aligned} \mu_p^{(SU_6)} \equiv -\frac{3}{2}\mu_n^{(SU_6)} &= \mu_p^{LO} \left[1 + \delta - \frac{23}{200} \left(\frac{g_A}{\pi F} \right)^2 \int_0^\infty dp p^4 \frac{F_{\pi NN}^2(p^2)}{w_\Phi^3(p^2)} \right] \\ &+ \frac{9}{50} m_N \left(\frac{g_A}{\pi F} \right)^2 \int_0^\infty dp p^4 \frac{F_{\pi NN}^2(p^2)}{w_\Phi^4(p^2)}. \end{aligned} \quad (78)$$

Taking into account the meson-in-flight diagram (Fig.3) generated by two-body forces leads to a deviation of the ratio μ_n/μ_p from the naive SU_6 result.

In general case, for our set of parameters we obtain:

$$\mu_p = 2.62 \pm 0.02, \quad \mu_n = -2.02 \pm 0.02, \quad \text{and} \quad \frac{\mu_n}{\mu_p} = -0.76 \pm 0.01 \quad (79)$$

where the range of theoretical predictions reflects the variation of the size parameter R . The separate LO (μ_p^{LO} , μ_n^{LO}) and NLO (μ_p^{NLO} , μ_n^{NLO}) contributions to the magnetic moments are given by

$$\begin{aligned} \mu_p^{LO} &= 1.8 \pm 0.15, \quad \mu_n^{LO} \equiv -\frac{2}{3}\mu_p^{LO}, \\ \mu_p^{NLO} &= \mu_p - \mu_p^{LO} = 0.82 \pm 0.13, \quad \mu_n^{NLO} = \mu_n - \mu_n^{LO} = -0.82 \pm 0.08. \end{aligned} \quad (80)$$

Our results for μ_p and μ_n are close to the ones of the chiral soliton quark model by Diakonov and Petrov [7]: $\mu_p = 2.98$ and $\mu_n = -2.26$. For the electromagnetic nucleon radii we obtain

$$\begin{aligned} r_E^p &= 0.84 \pm 0.05 \text{ fm}, \quad < r^2 >_E^n = -0.046 \pm 0.006 \text{ fm}^2, \\ r_M^p &= 0.82 \pm 0.02 \text{ fm}, \quad r_M^n = 0.85 \pm 0.01 \text{ fm}. \end{aligned} \quad (81)$$

The LO contributions to the charge radius of the proton (see Eq. (14)) and to the magnetic radii of proton and neutron are dominant

$$r_E^p \Big|_{LO} = 0.77 \pm 0.06 \text{ fm}, \quad r_M^p \Big|_{LO} \equiv r_M^n \Big|_{LO} = 0.73 \pm 0.06 \text{ fm}. \quad (82)$$

For the neutron charge radius squared we get the observed (negative) sign, but its magnitude is smaller than the experimental value. As in the naive $SU(6)$ quark model, the LO contribution to the neutron charge radius is zero and only one-loop diagrams give nontrivial contributions to this quantity: the meson-cloud (MC) $< r^2 >_{E;MC}^n = -0.072 \pm 0.006 \text{ fm}^2$

and vertex-correction (VC) $\langle r^2 \rangle_{E;VC}^n \approx 0.026 \text{ fm}^2$ diagrams. The total contribution to the neutron charge radius is given by

$$\langle r^2 \rangle_E^n = \langle r^2 \rangle_{E;MC}^n + \langle r^2 \rangle_{E;VC}^n = -0.046 \pm 0.006 \text{ fm}^2. \quad (83)$$

The magnitude of our result for the neutron charge radius, which is too small compared to the experimental value, is due to the reduced contribution of the pion cloud diagram (Fig.2c). The size of the meson cloud effects is in turn related to the magnitude of the renormalization constant, which for our model is $Z=0.9$ and therefore close to unity. With an increased contribution of the pion cloud, that is a decrease of Z , one is able to reproduce the experimental result for the neutron charge radius, but one also obtains a worse description of the magnetic moments and the proton charge radius. Also, perturbation theory up to one loop becomes less reliable in terms of good convergence properties. For example, choosing $\rho = 0.12$ (or $g_A = 1.5$) and $R = 0.52 \text{ fm}$ we obtain $\langle r^2 \rangle_E^n = -0.08 \text{ fm}^2$ and $\hat{Z} = 0.73$. However, for the other quantities we get a worse fit with: $\mu_p = 2.56$, $\mu_n = -2.18$, $r_E^p = 0.75 \text{ fm}$, $r_M^p = 0.9 \text{ fm}$ and $r_M^n = 1 \text{ fm}$. In comparison, the cloudy bag model [4] gets a value of $\langle r^2 \rangle_E^n = -0.14 \text{ fm}^2$ by an increased contribution of the pion cloud with $Z \approx 0.73$ [27]. As a result, the predicted values for the proton magnetic moment are also less satisfactory with $\mu_p = 2.2$ as in the original version of the cloudy bag model [4] and $\mu_p = 2.46$ in the improved version [27]. The prediction for the proton charge radius is also relatively small: $r_E^p = 0.73 \text{ fm}$ [4].

An improved fit to the neutron charge radius, while keeping the good results for the other static observables, can possibly be achieved by including center-of-momentum corrections and also Lorentz boost effects Refs. [4,5,30–37]), which are based on approximate techniques and are not included yet in the present evaluation. Furthermore, additional contributions of excited quark/antiquark states in the meson loop diagrams will further enhance the meson-cloud effects, which up to now were not studied yet consistently.

In Table I we summarize our results for the static electromagnetic properties of the nucleon in comparison with experimental data [38]. Finally, in Figs.4-8 we indicate the Q^2 -dependence of the electromagnetic form factors. In Fig.4 we present the result for the proton charge form factor at a typical value for the free size parameter $R = 0.6 \text{ fm}$. The dotted line corresponds to the LO result, the short-dashed line marks the NLO contribution, while the solid line corresponds to the total result at one loop. And, finally, the long-dashed line indicates the dipole fit to experimental data given by

$$G_D(Q^2) = \frac{1}{(1 + Q^2/0.71 \text{ GeV}^2)^2}. \quad (84)$$

The dependence of the proton charge form factor on the free parameter R is presented in Fig.5. We plot three curves corresponding to $R = 0.55 \text{ fm}$, $R = 0.6 \text{ fm}$ and $R = 0.65 \text{ fm}$. An increase of R leads to a decrease of the proton charge form factor and vice versa. In Fig.6 we give the results for the proton charge and the nucleon magnetic form factors for $R = 0.6 \text{ fm}$ and compare them with the common dipole fit. In Fig.7 we plot our predictions for the ratio $\mu_p G_E^p(Q^2)/G_M^p(Q^2)$ at $R = 0.6 \text{ fm}$ and compare them with experimental data taken from [39] and [40]. Our predictions for the ratio $G_M^n(Q^2)/(\mu_n G_D(Q^2))$ are presented in Fig.8. Experimental data are taken from [41]- [44]. Finally, in Fig.9 we plot the results for the neutron charge form factor at different values of R : $R = 0.55 \text{ fm}$, $R = 0.6 \text{ fm}$ and $R = 0.65 \text{ fm}$. Our results are lower than the experimental points taken from Refs. [45]- [49].

IV. SUMMARY AND CONCLUSIONS

In this paper, we have considered the perturbative chiral quark model (PCQM) based on an effective chiral Lagrangian which includes confinement phenomenologically. The Lagrangian basically describes nucleons as bound states of three valence quarks surrounded by a perturbative cloud of pseudoscalar mesons as dictated by the chiral symmetry requirement.

The main aim of this investigation was to present a consistent formalism when treating the Lagrangian in the one-loop expansion. We thereby employed a technique, which by appropriate introduction of counterterms allows consistent mass renormalization both on the quark and the nucleon level. In a further extension of the PCQM we considered the coupling of the photon field to the nucleon. Again, charge renormalization was introduced to keep a proper definition of the nucleon charge. Local gauge invariance of the electromagnetic interaction is fulfilled on the Lagrangian level by construction. Due to the noncovariant nature of the effective confinement we introduced, local gauge invariance is not necessarily fulfilled for physical amplitudes in any reference frame. Only when working in the Breit frame, nucleon matrix elements were shown to be consistent with the Ward identity without further need to introduce extra terms, like contact interactions, in the Lagrangian.

As one basic application of the developed formalism we considered the electromagnetic form factors of the nucleon. Two approximations were introduced:

- i) restriction of the relativistic quark states to the ground state, that is N and Δ intermediate states occur in the one-loop terms;
- ii) Gaussian form of the ground state single quark wave function, modelled for low- Q^2 physics of the calculated observables.

The derived quantities (magnetic moments, radii and form factors) contain only one model parameter R , which is related to the radius of the three-quark core, and are otherwise expressed in terms of fundamental parameters of low-energy hadron physics: axial coupling constant g_A , weak pion decay constant F and set of QCD parameters (current quark masses \hat{m} and m_s and quark condensate parameter B). Predictions are given for a variation of the free parameter R in a physical region from 0.55 fm to 0.65 fm corresponding to $\langle r_E^2 \rangle_{3q-core}^P$ ranging from 0.5 fm² to 0.7 fm². Our low Q^2 results, that is for the nucleon magnetic moments, the charge radius of the proton and the magnetic radii of the nucleons are in reasonable agreement with data, strengthening the phenomenological validity of the PCQM. For the charge radius of the neutron we obtain the correct sign but its magnitude is smaller than the experimental value.

We also presented a detailed discussion of the Q^2 -dependence of the nucleon form factors in the space-like region. Although the model underestimates the finite Q^2 behaviour of the form factors, certain additional physics aspects, such as c.m. correction and Lorentz boost effects, are known to improve the phenomenological fit (see detailed discussion in Refs. [4,5,30–37]). The issue of c.m. corrections as evaluated in the PCQM machinery and their consistency with the chiral expansion of the nucleon mass will be addressed in a forthcoming publication. With the formal and phenomenological foundation established, the proposed model serves as a basis for further applications to recent issues of nucleon structure, for example such as photo- and electroproduction of pseudoscalar mesons, which will be pursued in future.

Acknowledgements. This work was supported by the Deutsche Forschungsgemeinschaft (DFG, grant FA67/25-1).

REFERENCES

- [1] Proc. 8th Int. Symp. “Meson-Nucleon Physics and the Structure of the Nucleon (MENU 99)”, Zuoaz, Switzerland, 16-20 Aug 1999. πN Newslett. (1999) No. 15.
- [2] Proc. Workshop 8th “Structure of Nucleon (NUCLEON 99)”, Frascati, Italy 7-9 June 1999, Eds. E. De Santis et al. Nucl. Phys. A 666-667 (2000).
- [3] Proc. of 8th Int. Conf. ”Baryons-98”, Bonn, Germany, 22-26 Sep 1998, World Sci. Publ. (1999), Eds. D.W. Menze and B.Ch. Metsch.
- [4] S. Théberge, A. W. Thomas, and G. A. Miller, Phys. Rev. D **22**, 2838 (1980); Phys. Rev. D **24**, 216 (1981); S. Théberge and A. W. Thomas, Nucl. Phys. **A393**, 252 (1983); A.W. Thomas, Adv. Nucl. Phys. **13**, 1 (1984).
- [5] E. Oset, R. Tegen, and W. Weise, Nucl. Phys. **A426**, 456 (1984); R. Tegen, Ann. Phys. **197**, 439 (1990) 439.
- [6] S. A. Chin, Nucl. Phys. **A382**, 355 (1982).
- [7] D. Diakonov and V. Yu. Petrov, Nucl. Phys. **B245**, 259 (1984); Nucl. Phys. **B272**, 457 (1986); D. Diakonov, V. Yu. Petrov, and P. V. Pobilitza, Nucl. Phys. **B306**, 809 (1988); D. I. Diakonov, V. Yu. Petrov, and M. Praszalowicz, Nucl. Phys. **B323**, 53 (1989).
- [8] T. Gutsche and D. Robson, Phys. Lett. **B229**, 333 (1989); T. Gutsche, Ph. D. Thesis, Florida State University, 1987 (unpublished).
- [9] A. Chodos, R. L. Jaffe, K. Johnson, C. B. Thorn and V. F. Weisskopf, Phys. Rev. **D9**, 3471 (1974).
- [10] V. E. Lyubovitskij, T. Gutsche, A. Faessler, and E. G. Drukarev, Phys. Rev. **D63**, 054026 (2001).
- [11] M. Lüscher, Nucl. Phys. **B180**, 317 (1981).
- [12] T. T. Takahashi, H. Matsufuru, Y. Nemoto, and H. Suganuma, Phys. Rev. Lett. **86**, 18 (2001).
- [13] M. Gell-Mann, M. Lévy, Nuovo Cim. **16**, 1729 (1960).
- [14] J. Gasser, H. Leutwyler, and M. E. Sainio, Phys. Lett. **B253**, 252, 260 (1991).
- [15] P. M. Gensini, Preprint DFUPG-98-GEN-02, 1998.
- [16] A. L. Fetter and J. D. Walecka, Quantum Field Theory of Many-Particle Systems, McGraw-Hill Publ., 1971.
- [17] J. Gasser, M. E. Sainio, and A. B. Švarc, Nucl. Phys. **B307**, 779 (1988).
- [18] S. Weinberg, Physica **A96**, 327 (1979). J. Gasser and H. Leutwyler, Ann. Phys. (N.Y.) **158**, 142 (1984); Nucl. Phys. **B250**, 465 (1985).
- [19] J. Gasser and H. Leutwyler, Phys. Rep. **87**, 77 (1982).
- [20] I. Duck, Phys. Lett. **B77**, 223 (1978).
- [21] M. Gell-Mann and F. Low, Phys. Rev. **84**, 350 (1951).
- [22] N. N. Bogoliubov and D. V. Shirkov, An Introduction to Theory of Quantized Fields (Wiley-Interscience, New York, 1959).
- [23] F. E. Close, An Introduction to Quarks and Partons (Academic Press, New York, 1979).
- [24] F. J. Ernst, R. G. Sachs and K. C. Wali, Phys. Rev. **119**, 1105 (1960).
- [25] R.G. Sachs, Phys. Rev. **126**, 2256 (1962).
- [26] G. A. Miller and A. W. Thomas, Phys. Rev. **C56**, 2329 (1997).
- [27] D. H. Lu, A. W. Thomas and A. G. Williams, Phys. Rev. **C57**, 2628 (1998).
- [28] M. A. Ivanov, M. P. Locher, V. E. Lyubovitskij, Few Body Syst. **21**, 131 (1996).
- [29] A. W. Thomas and G. Krein, Phys. Lett. **B456**, 5 (1999).

- [30] A. L. Licht and A. Pagnamenta, Phys. Rev. **D6**, 1150, 1156 (1970).
- [31] D. P. Stanley and D. Robson, Phys. Rev. **D26**, 223 (1982).
- [32] I. Picek and D. Tadić, Phys. Rev. **D27**, 665 (1983).
- [33] W.-Y. P. Hwang, Z. Phys. **C16**, 327 (1983).
- [34] P. A. M. Guichon, Phys. Lett. **B129**, 108 (1983).
- [35] S. Kuroda, K. Fujii, M. Bando and T. Okazaki, Phys. Lett. **B146**, 83 (1984).
- [36] H. R. Fiebig and E. Hadjimichael, Phys. Rev. **D30**, 181, 195 (1984).
- [37] E. G. Lübeck, E. M. Henley and L. Willets, Phys. Rev. **D35**, 2809 (1987).
- [38] D. E. Groom et al, Eur. Phys. J. **C15**, 1 (2000).
- [39] M. K. Jones et al, Phys. Rev. Lett. **84**, 1398 (2000).
- [40] B. D. Milbrath et al, Phys. Rev. Lett. **80**, 452 (1998); Phys. Rev. Lett. **82**, 2221(E) (1999).
- [41] P. Markowitz et al, Phys. Rev. **C48**, R5 (1993).
- [42] H. Anklin et al, Phys. Lett. **B366**, 313 (1994).
- [43] E. E. W. Bruins et al, Phys. Rev. Lett. **75**, 21 (1995).
- [44] H. Anklin et al, Phys. Lett. **B428**, 248 (1998).
- [45] M. Ostrick et al, Phys. Rev. Lett. **83**, 276 (1999).
- [46] J. Becker et al, Eur. Phys. J. **A6**, 329 (1999).
- [47] M. Meyerhoff et al, Phys. Lett. **B327**, 201 (1994).
- [48] T. Eden et al, Phys. Rev. **C50**, R1749 (1994).
- [49] S. Platchkov et al, Nucl. Phys. **A510**, 740 (1990).

TABLES

Table I. Static nucleon properties.

Quantity	Our Approach	Experiment [38]
μ_p	2.62 ± 0.02	2.793
μ_n	-2.02 ± 0.02	-1.913
$\frac{\mu_n}{\mu_p}$	-0.76 ± 0.01	-0.68
r_E^p (fm)	0.84 ± 0.05	0.86 ± 0.01
$\langle r^2 \rangle_E^n$ (fm ²)	-0.046 ± 0.006	-0.119 ± 0.004
r_M^p (fm)	0.82 ± 0.02	0.86 ± 0.06
r_M^n (fm)	0.85 ± 0.01	0.88 ± 0.07

FIGURES

Fig.1: Diagrams contributing to the baryon energy shift: meson cloud (1a) and exchange diagram (1b).

Fig.2: Diagrams contributing to the nucleon charge: triangle diagram (2a), triangle counterterm diagram (2b), meson-cloud diagram (2c), vertex correction diagram (2d), self-energy diagrams (2e) and (2f), self-energy counterterm diagrams (2g) and (2h), exchange current diagrams (2i) and (2j) and exchange current counterterm diagrams (2k) and (2l).

Fig.3: Meson-in-flight diagram.

Fig.4: Proton charge form factor: LO, NLO and Total contributions.

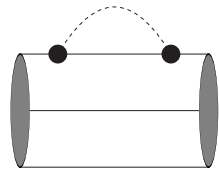
Fig.5: Proton charge form factor for different values of the 3q-core radius $R = 0.55, 0.6$ and 0.65 fm.

Fig.6: Proton charge and nucleon magnetic form factors at $R = 0.6$ fm.

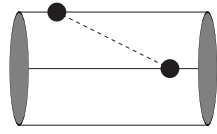
Fig.7: The ratio $\mu_p G_E^p(Q^2)/G_M^p(Q^2)$ at $R = 0.6$ fm. Experimental data are taken from [39] (JLAB) and [40] (MIT-Bates).

Fig.8: The ratio $G_M^n(Q^2)/(\mu_n G_D(Q^2))$ at $R = 0.6$ fm. Experimental data are taken from [41] (MIT-Bates), [42] (NIKHEF), [43] (ELSA) and [44] (MAMI).

Fig.9: Neutron charge form factor for different values of $R = 0.55, 0.6$ and 0.65 fm. Experimental data are taken from [45] (MAMI-1), [46] (MAMI-2), [47] (MAMI-3), [48] (MIT) and [49] (PARIS).

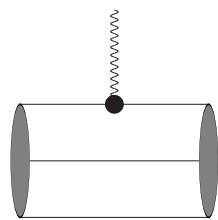


(a)

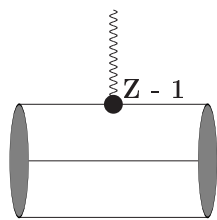


(b)

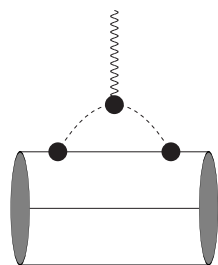
Fig.1



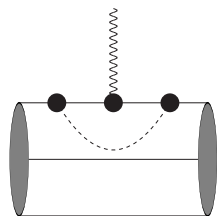
(a)



(b)

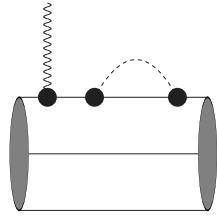


(c)

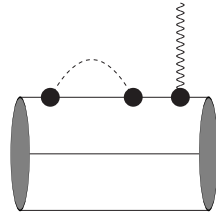


(d)

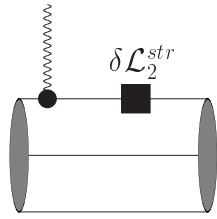
Fig.2



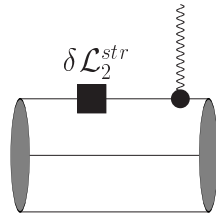
(e)



(f)

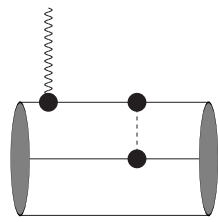


(g)

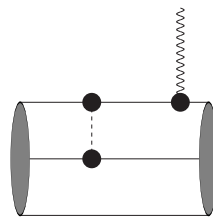


(h)

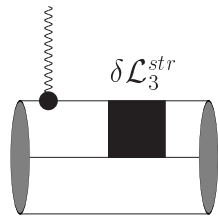
Fig.2 (continue)



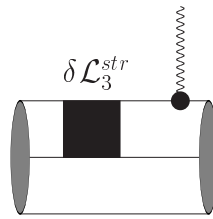
(i)



(j)



(k)



(l)

Fig.2 (continue)

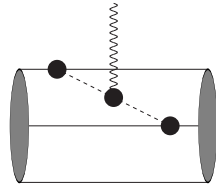


Fig.3

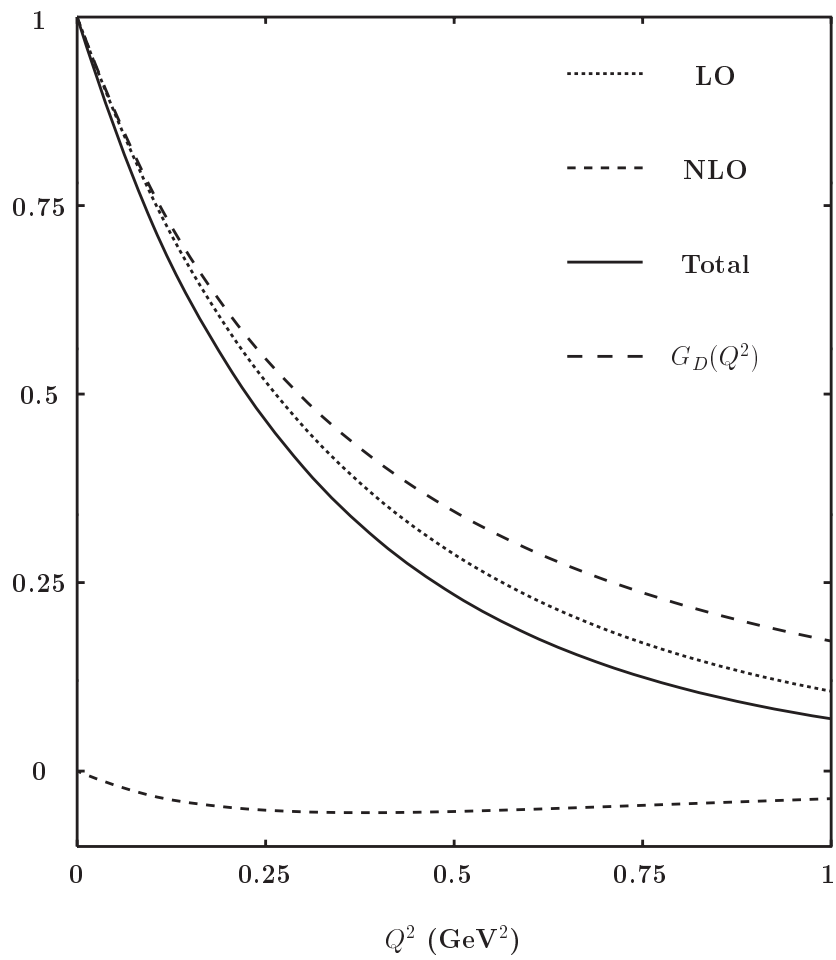


Fig.4

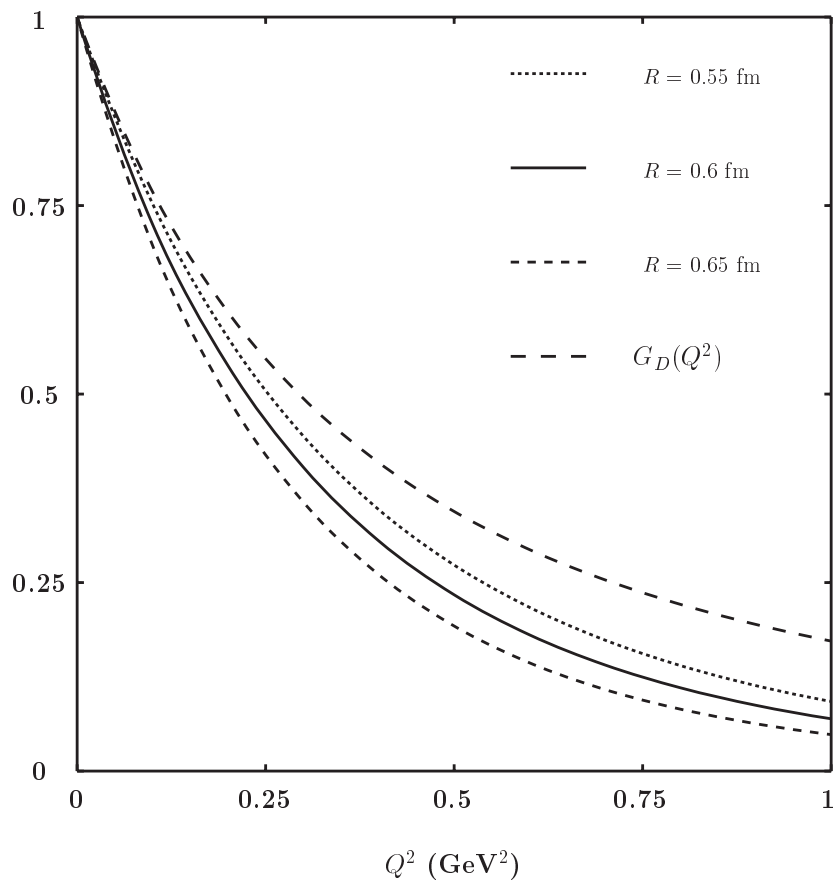


Fig.5

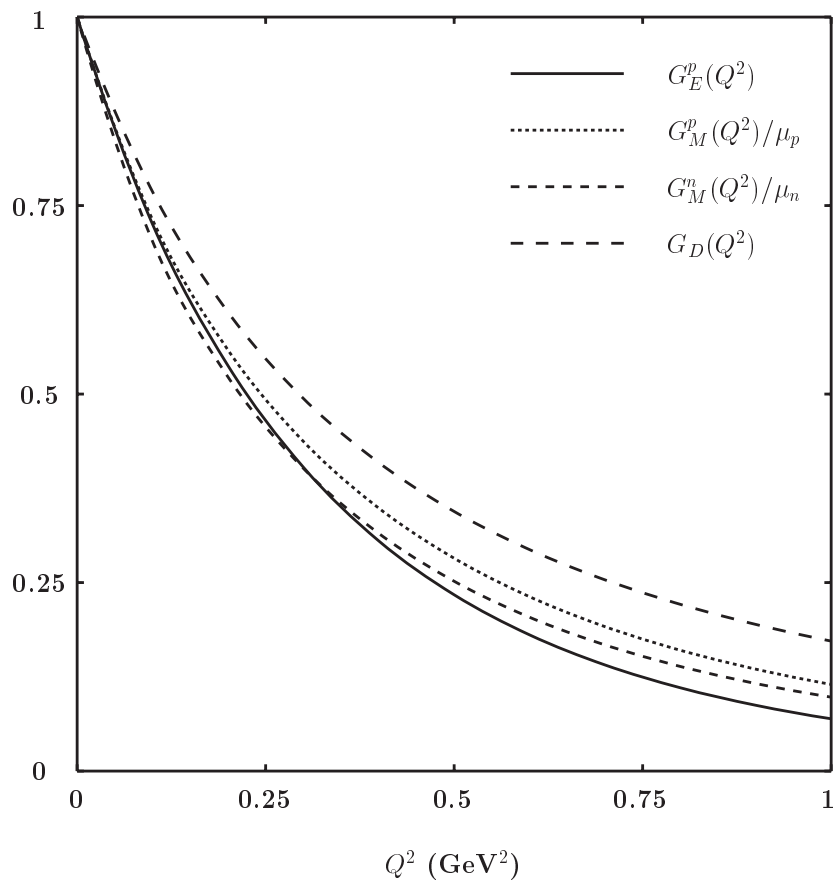


Fig.6

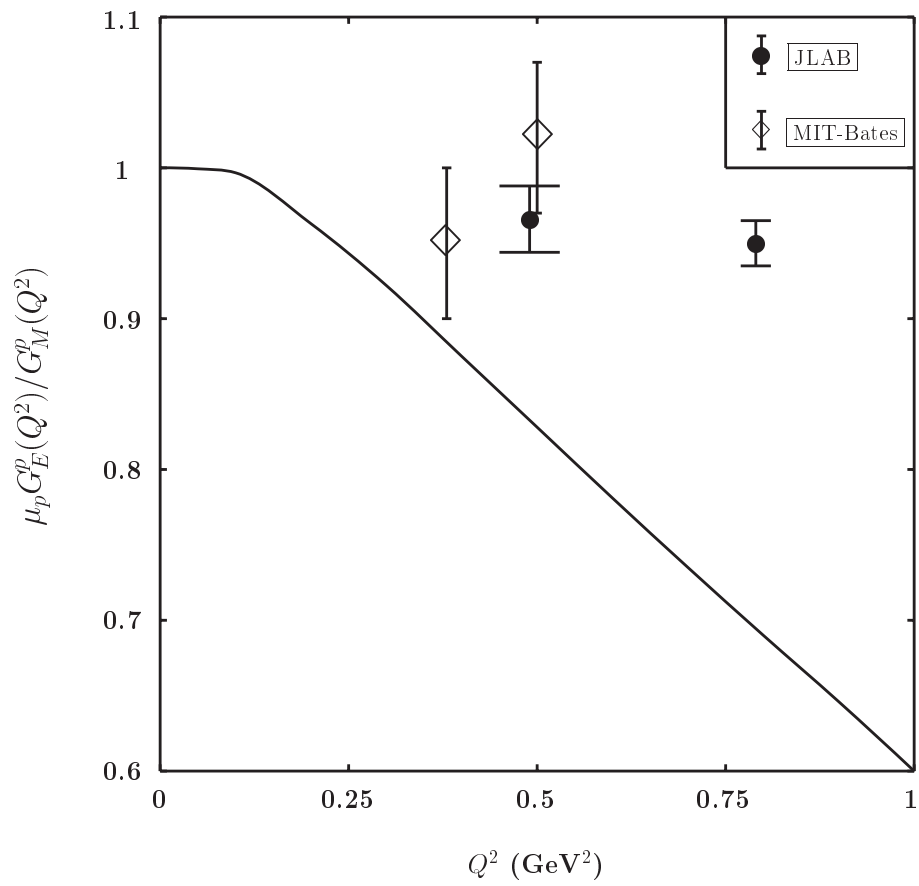


Fig.7

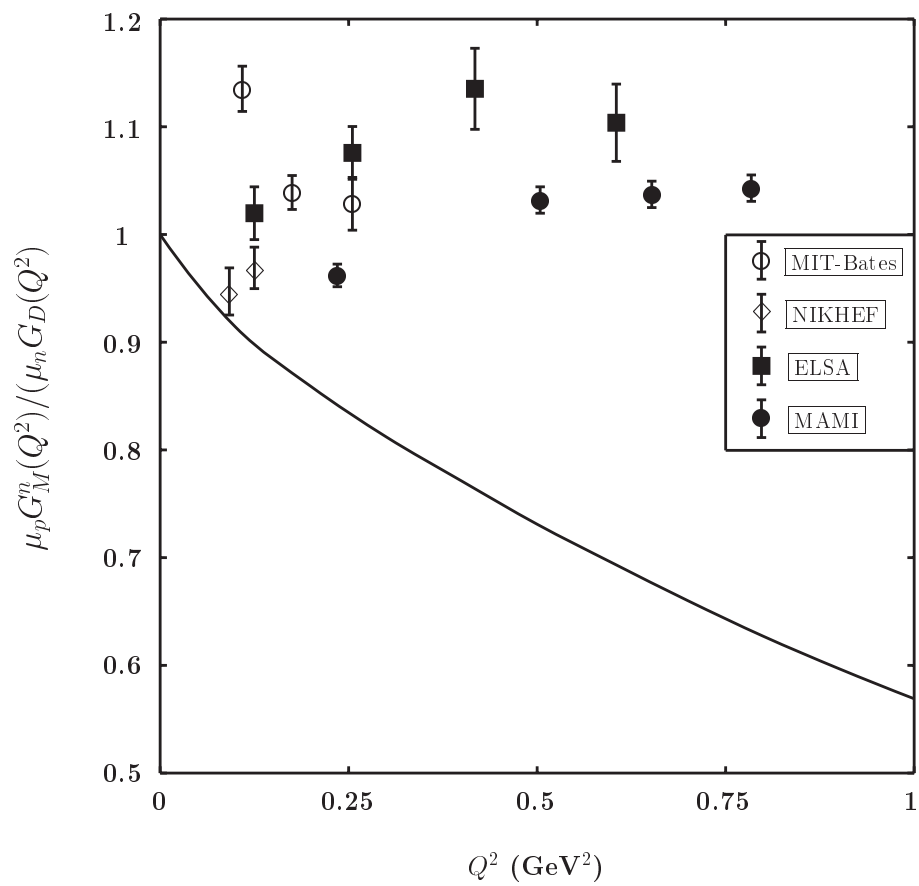


Fig.8

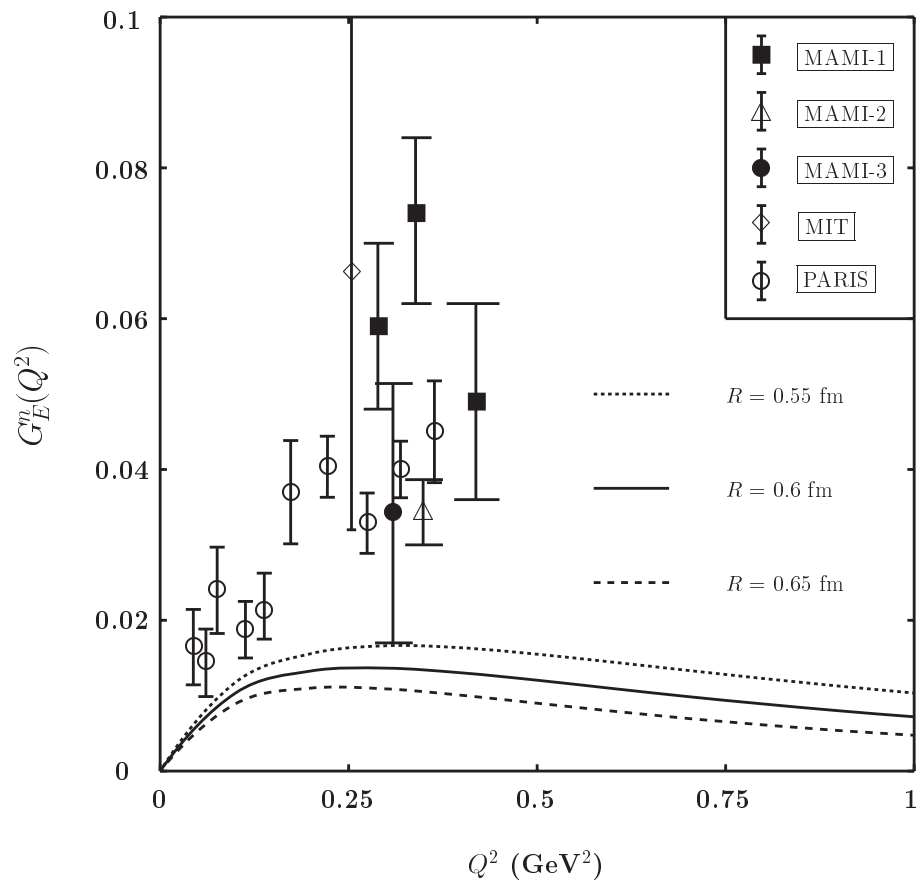


Fig.9